PARAMETRIC AND KINETIC STUDY OF NITRATE REMOVAL FROM WATER BY MODIFIED CHITOSAN COMPOSITE BEADS

Zainab N. Jamka[1,✉], Wadood T. Mohammed[1]

Abstract. The contamination of water bodies with harmful pollutants considers an aggravating global problem. The current research focuses on a developing efficient adsorbed for removing nitrate ions from aqueous solutions. The study proposed modified chitosan-zeolite composite beads to enhance the performance of the adsorption process. The zeolite was used to increase the surface area, and Zirconium was loaded on the beads to promote the selectivity for nitrate anions. The adsorption mechanism was assessed by characterizing the beads and sorbate adsorbent beads utilizing X-ray diffraction analysis (XRD), Fourier transform infrared spectroscopy (FTIR), Field Emission Scanning Electron Microscopy (FESEM), and analysis with an energy dispersive X-ray analyzer (EDX). The experiments were conducted in a batch system, and the effect of key parameters like contact time, initial nitrate anion concentration, and adsorbent dosage on the adsorption performance was investigated. The results demonstrated that the highest removal of nitrate ions was determined to be 95.42% at 0.2 g of Cs-Ze-Zr adsorbent with an initial concentration of 50 mg/L and a contact time of 120 minutes. The maximum adsorption capacity of the nitrate ions on the manufactured bead was 80.15 mg/g. In addition, among the Freundlich, Langmuir, and Temkin isotherms, the isotherm equilibrium data were consistent with a Freundlich isotherm model. The kinetic data for adsorption were satisfactorily fitted by a pseudo-first order. Subsequently, the results distinctly indicated that the proposed adsorbed (Cs-Ze-Zr) could be employed fruitfully in removing nitrate ions, demonstrated through the remarkable removal efficiency and adsorption capacity obtained in the study.

Keywords: modified chitosan, batch adsorption, nitrate, zeolite, zirconium.

1. Introduction

Water considers the essence of life. Unfortunately, controlling the quality of water is a foremost challenge. Water is infested by several wastes, including industrial, agricultural, biological, and other dispersed sources.[1]

A wide variety of harmful ions can be presented in water sources. Nitrate ions have attracted more attention as a straightforward problem arises in this domain. Nitrate ions are characterized by high levels of water solubility and may inflict serious and long-term environmental and human health harm. It may cause carcinogenic diseases and the development of nitrosamines and nitrosamide.[2,3] Accordingly, substantial interest has been received to find a sufficient technology to remove the anionic pollutant from the water resources. Over the last few decades, the researcher has developed different approaches, including chemical, physical and biological treatments such as a membrane technology,[4] electrocoagulation reduction,[5] reverse osmosis,[6] precipitation,[7] catalytic reduction,[8] and other technologies.

Adsorption has been proposed as a viable technique for wastewater treatments as it represents a simple, flexible, and sustainable method.[9] The basic fundamental of this technology involves the mass transfer process in which the dissolved substance is emigrated from the bulk of fluid to the surface of the adsorbent by means of chemical and/or physical interaction.[10,11]

It has been recognized that the type of adsorbent plays a crucial role in the adsorption process. Numerous studies suggest various adsorbents, including organic adsorbents, inorganic adsorbents, and agricultural wastages such as activated carbon,[12] silica gel,[13] and dates pits.[14]

Recently, chitosan has been addressed as one of the adsorbents used successfully in removing toxic ions.[15] It is obtained from chitin by deacetylation and consists of a linear polysaccharide, which considers one of the superior abundant biopolymeric materials. This type of adsorbent offers some practical advantages compared to other adsorbents, which can be summarized as a biomaterial that can be formed into different shapes, biodegradability, and biocompatibility.[16] Also, the primary advantage of chitosan is that it has a high content of amino and hyd-

[1] Chemical Engineering Department, University of Baghdad,
Baghdad, Iraq
✉ *zainab.mohammed1607m@coeng.uobaghdad.edu.iq*

roxyl groups and the amino groups which tolerate protonation readily in an acidic medium.[17] Despite the mentioned advantages of chitosan, some drawbacks are pointed out through utilizing chitosan, including poor selectivity and adsorption capacity, low mechanical strength, and low level of solubility in an acidic environment.[18] Consequently, recent approaches focus on overcoming these problems by proposing different modification methods to enhance chitosan's physicochemical properties of chitosan.[19] These methods can be classified into physical and chemical modifications, such as composite blend forms,[20] metal loading,[21] and crosslinking.[22]

Many alternative approaches have been adopted to improve the properties of adsorbents, like removal efficiency and adsorption capacity. One way to overcome this problem is to load it with other substances, for instance, multivalent metal ions. Anions like nitrite are more likely to be removed by ions with a higher positive charge, such as Calcium, Magnesium, Aluminum and Lanthanum ions.[23] Zirconium has a higher positive charge among various types of ions and is biologically and chemically inert. This material is resistant to oxidant and reductant, alkalis, and acids.[24]

Moreover, zeolites are characterized by a relatively high specific surface area and ion exchange capacity. Zeolites are negative-charged hydrated aluminosilicate minerals.[25] The empirical chemical formula for zeolite can be expressed as $M_{2/n}O. Al_2O_3.ySiO_2. wH_2O$.[26]

The main objective of the current study is to cast a new light on the removal of nitrate ions from an aqueous medium by adsorption using modified adsorbents. For this purpose, chitosan was modified by mixing with zeolites, and the final mixture was loaded with Zirconium. The synthesized modified adsorbents were characterized and used in the batch adsorption process. The study questions the feasibility of utilizing the modified chitosan adsorbents in the adsorption process regarding removal efficiency and adsorption capacity. Therefore, the effect of key parameters, specifically contact time, the concentration of pollutant and the dose of adsorbent were examined in this work. In addition, the study involved introducing different adsorption isotherms for the process and adopting the kinetic model that fits the adsorption mechanism.

2. Experimental

2.1. Chemicals

Chitosan powder (90% deacetylated) was purchased from chemsavers (USA), 13X zeolite powder from ZR CATALYST CO.LTD (China), zirconium chloride ($ZrOCL_2.8H_2O$) from BDH chemicals Ltd England, glacial acetic acid (99.5%) from MACRON (China), glutaraldehyde solution (25%) from THOMAS BAKER, sodium hydroxide pellets (98%) from ORBITAL company, sodium nitrate ($NaNO_3$) is supplied by CDH. Distilled water was used to prepare all solutions.

2.2. Preparation Chitosan-Zeolite (Cs-Ze-Zr) Beads

The chitosan-zeolite beads were created using a previously reported method by Sowmya and Meenakshi[27] with modifications. Two grams of chitosan were dissolved in 100 mL of glacial acetic acid (2% v\v) in a 250 mL beaker. The mixture was stirred by a mixer (OS20-S) for three hours at 300 rpm in ambient temperature to obtain the homogenous gel. Then 0.5g of 13X zeolite was added to the chitosan mixture and mixed for two hours.[28]
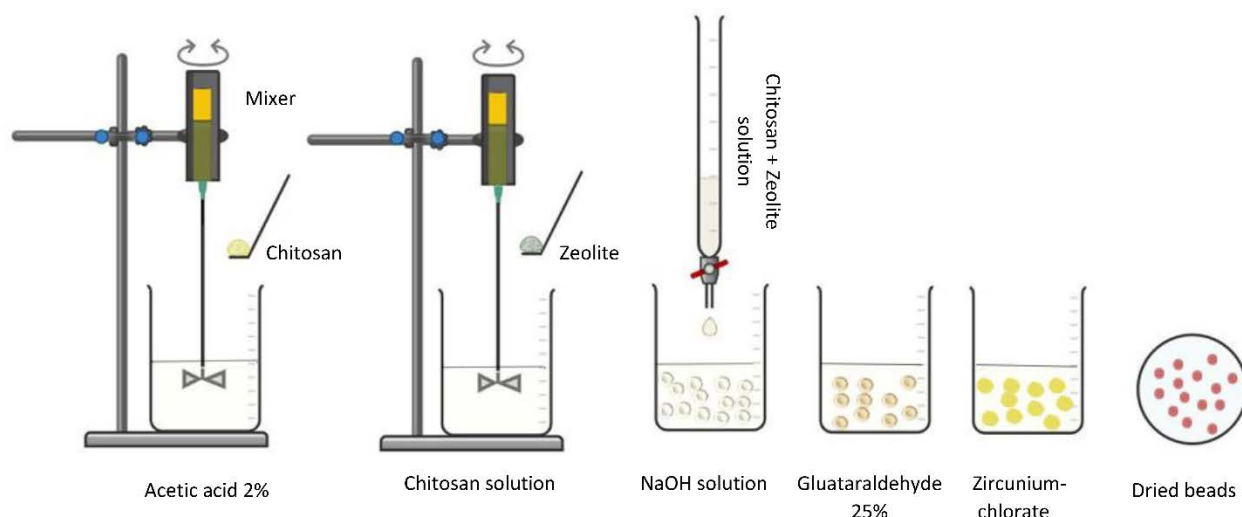

Fig. 1. Shedule of modified chitosan composite beads Cs-Ze-Zr preparation

Chitosan and zeolite solution was dropped in a beaker (1L) containing 1M sodium hydroxide by burette (100 mL) and left for 20 h to obtain viscous beads. After that, the beads were washed with distilled water until the pH value reached 6.5-7.0, after that the wet beads were immersed in a glutaraldehyde solution (25%, 48hour) and washed with distilled water to neutralize pH. Finally, the (Cs-Ze) wet beads were placed in zirconium chloride solution (ZrOCL$_2$.8H$_2$O, 5%w/v) for 24 h and then washed several times with distilled water to remove the excess zirconium chloride. The beads were dried at room temperature as shown in Fig. 1.

2.3. The Batch Adsorption Experiments

The batch adsorption experiments were performed in a 250 mL glass bottle placed in a flask shaker (1990-Germany). A specific amount of the prepared (Cs-Ze-Zr) adsorbents was placed in 250 ml of sodium nitrate solution. The mixture was shaken at a constant rotation speed of 150rpm at room temperature.

The effect of contact time (0–180 min), adsorbent dosage (0.05-0.3g), and initial nitrate ions (50-600 mg/L) on a removal efficiency and adsorption capacity were investigated through the study. Samples were taken periodically and filtered before analysis. Thereafter, the samples were analyzed by a spectrophotometer at a wavelength of 220 nm according to the method described in the literature.[29]

The removal efficiency (removal %) is estimated according to the following Equation:

$$removal\ \% = 100 \cdot \frac{c_i - c_t}{c_i} \qquad (1)$$

where c_i is initial concentration of NO$_3$, c_t the concentration with time.

The adsorption capacity was calculated as follows:

$$adsorption\ capacity = \frac{c_i - c_t}{m} \cdot v \qquad (2)$$

where m is mass of adsorbent, v volume of solution.

3. Results and Discussion

3.1. Cs-Ze-Zr beads

The adopted preparation method of (Cs-Ze-Zr) beads gives substantial results interpreted in Fig. 2. As can be observed from the pictures, the first step of preparation gives viscous white beads of chitosan-zeolite beads after they immersed in NaOH solution as in (2-A). In the second step, the beads turned into semi-solid beige beads after they were treated with glutaraldehyde, as in (2-B). Thereafter, the exposition of beads to zirconium chloride solution made the bead's color yellow, as shown in (2-C). Finally, the beads gain their ultimate dark brown color after drying as in (2-D).

| A | B | C | D |

Fig. 2. Pictures of the beads obtained in each step of preparation Cs-Ze-Zr beads

3.2. XRD Analysis

The XRD spectra of chitosan, zeolite, Zirconium, and the composite Cs-Ze-Zr beads after adsorption are presented in Fig. 3. As can be observed, the XRD pattern of chitosan can be identified clearly from peaks that appear at 2θ of 20.34 and weaker peaks at 21.35 and 35.4, which is munching typical fingerprints of chitosan.[30,31] The test points out a high crystallinity with an average crystallite size of 9.8 nm for chitosan. The phase I.D. of the XRD pointed that zeolite can be characterized by broad peaks at 2θ of 6.04, 9.95, 15.4, 23.3 and 30.9. The pointed peaks demonstrated the amorphous nature of 13X zeolite.[32-34]

Additionally, the XRD diffraction patterns for Zirconium were located at 2θ of 7.4, 14.88, 23.43, 27.74 and 29.76. These peaks are also pointed according to ICSD 00-032-1498.[34] Furthermore, low-intensity peaks of XRD spectra for the composite Cs-Ze-Zr beads were located at 2θ of 5.9, 21.2, 20.7, 24.5, 31.6, and 39.5, which indicate the presence of chitosan, zeolite, and Zirconium with a small shift of their location. The Cs-Ze-Zr beads after adsorption declined in intensity after due to nitrate adsorption. The nitrate alters the surface structure of Cs-Ze-Zr beads. That behavior was also obtained when Fe-Cs-Alg beads were exposed to adsorption with phosphate.[15]

3.3. FTIR Studied of Adsorbent

FTIR spectra of chitosan (Cs), zeolite, (Cs-Ze-Zr) bead before and after adsorption are shown in Fig. 4. A broadband peak was observed, which was designated for the pure chitosan overlapped stretching vibrations of the -OH and NH$_2$ groups at 3444 cm^{-1}. The -CH$_2$ group's asymmetric C-H stretching vibrational peak was presented at 2862 cm^{-1}. Also, it can be noticed that the N-H bending vibration of NH$_2$ and -OH was 1577 and 1381 cm^{-1}. [15] Furthermore, the C-O-C skeletal vibrations caused the peak at 1076 cm^{-1}, while the C-O stretching vibration of chitosan caused the peak at 1026 cm^{-1}. [35] In the zeolite, the TO4 [36] (T = Si or Al) tetrahedral symmetric and asymmetric stretching vibrations, respectively, were represented by the peaks centering at 999 and 671 cm^{-1}. The building blocks of the octahedral structures were attributed to the dual six-member rings at 563 cm^{-1}. [37,36] The T-O bending vibration of the zeolite interior (where T = Al or Si) may be responsible for the absorption band at 463 cm^{-1}. [38] Additionally, it was possible to observe the Si(Al)-O vibration peak at 756 cm^{-1}. [39] Due to the presence of hydroxyl groups, the spectrum of 13X zeolite displayed a broad absorption band with a center at 3460 cm^{-1} that corresponded to OH vibrations. Before adsorption, the peak observed at 447 cm^{-1} [40] was attributed to the Zr-O bonds. The bands at 1670 cm^{-1} and 1577 cm^{-1} in chitosan shifted to 1651 cm^{-1} and 1539 cm^{-1} in Cs-Ze-Zr beads, which were attributed to intermolecular interaction between chitosan's -NH2 group and the Si-O and Al-O groups of the zeolite. The band appeared at 3444 cm^{-1} in chitosan reduced to 3360 cm^{-1} in Cs-Ze-Zr

bead. However, this peak reduced to 3082 cm^{-1} in Cs-Ze-Zr beads after adsorption, that may contributed to metal coordination with the chitosan functional groups. [2] In addition, spectra of beads after adsorption showed that a new peak at 1388 cm^{-1} [41] was related to the N-O stretching frequency, which demonstrated that nitrate ions had been adsorbed on the adsorbent.

3.4. FESEM and EDAX studies of adsorbent

Figure 5 (A-D) depicts FESEM images of Cs-Ze-Zr composite beads both before and after the adsorption of nitrate ions. Figures A&B show the spherical form of Cs-Ze-Zr prior to adsorption and the heterogeneous surface morphology with an extended roughness. The possibility of pollutants being absorbed is encouraged by the surface's rising roughness. The beads in figures C &D, after nitrate ion adsorption, still maintained their spherical shape, and the surface was smoother than it was before adsorption. This occurred because the nitrate ions had coated the beads after adsorption. Fig. 5E of EDAX spectra for Cs-Ze-Zr beads showed that the peak of Zr^{+4} obviously appeared, and this proved that the Zr^{+4} was successfully loaded onto the chitosan-zeolite beads. The rise in nitrogen weight percentage from 7.15% to 8.10% and oxygen atom weight percentage from 22.77% to 24.87%, as depicted in Fig. 5F, demonstrated the adsorption of nitrate ions on Cs-Ze-Zr composite beads. In addition, the chloride element was reduced compared with Fig. 5E, suggesting that the ion exchange mechanism also controlled the sorption system.
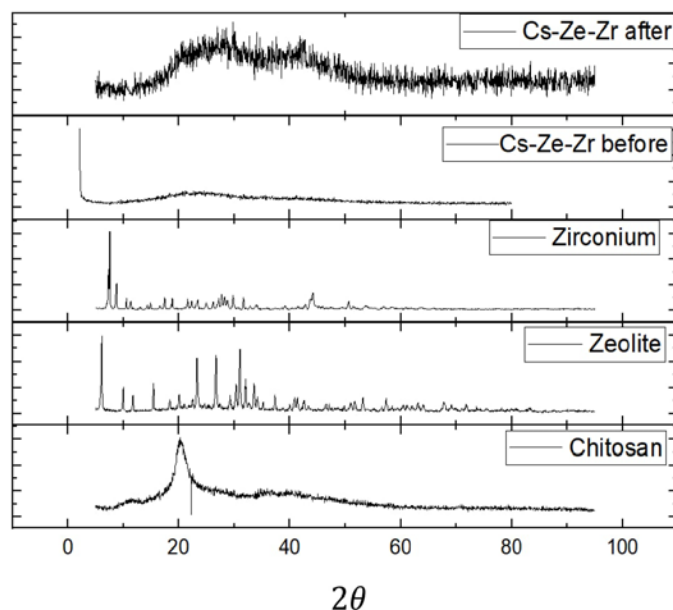

Fig. 3. XRD analysis of chitosan, zeolite, zirconium, and the composite Cs-Ze-Zr beads
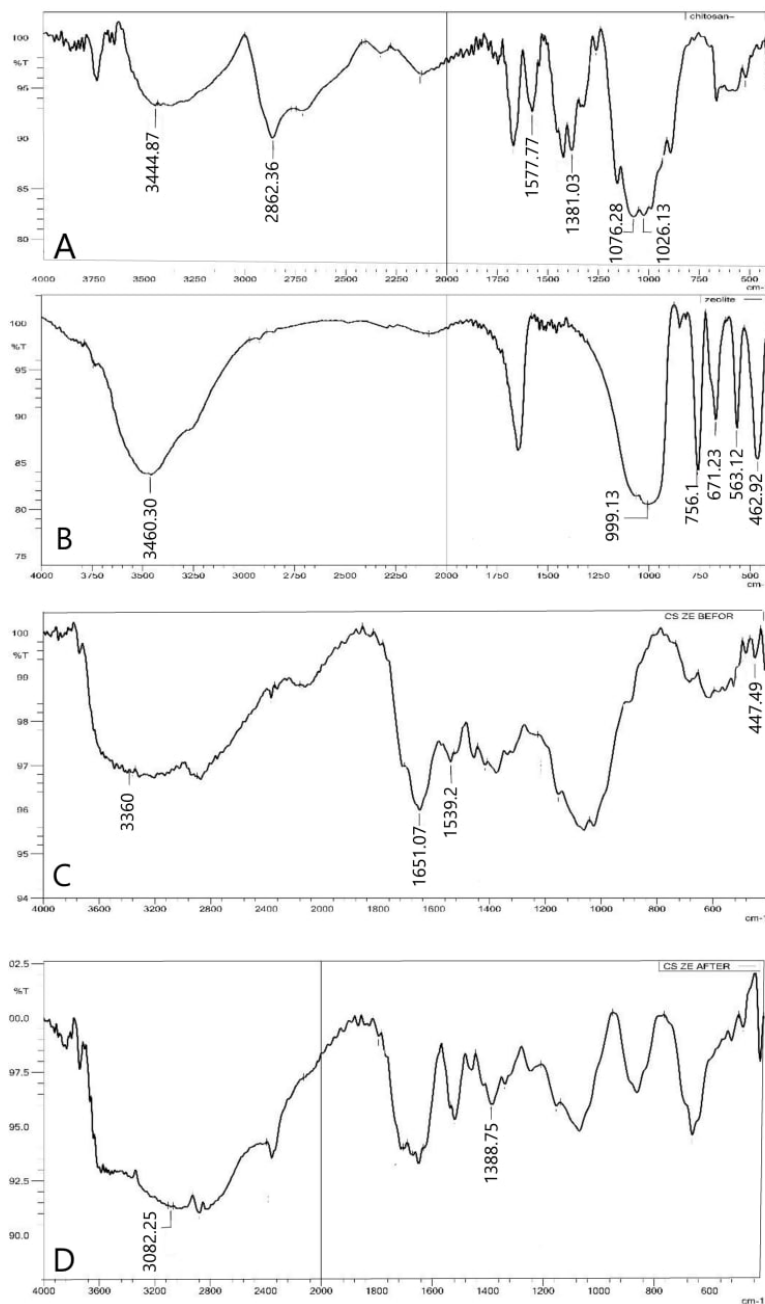
Fig. 4. FTIR spectra of (A) chitosan, (B) 13x zeolite, (C) Cs-Ze-Zr beads
before adsorption, and (D) Cs-Ze-Zr beads after adsorption

3.5. Effect of Contact Time

The effect of contact time on removal efficiency and adsorption capacity was examined with initial NO_3 concentration of 50 mg/L and an adsorbent dosage of 0.1 g. Fig. 6 shows that both removal efficiency and adsorption capacity increased with the contact time. The removal efficiency increased dramatically from 17% to 83% by increasing the time of adsorption from 30 min. to 120 min. After that, the removal efficiency starts to level off, where the increase of contact time to 180 minutes resulted in raising the efficiency only to 91.4%.

Similar behavior was observed with adsorption capacity. The adsorption capacity increased gradually from 4.27 mg/g to 20.7 mg/g with increased contact time from 30 to 120 minutes. The improvement of adsorption capacity was insignificant when the contact time exceeded 120 min, and reached about 22.6 mg/g at contact time of 180 minutes.
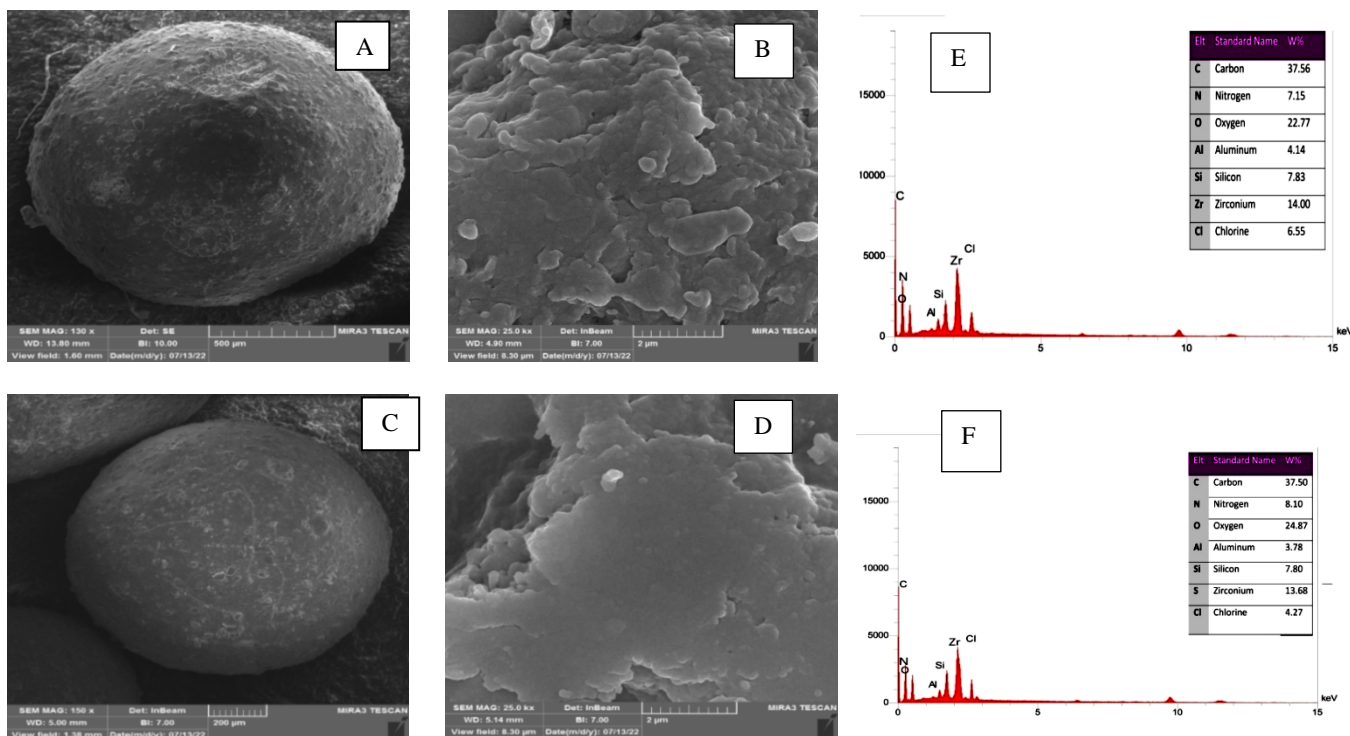
Fig. 5. Fesem images of (A, B) Cs-Ze-Zr beads before nitrate adsorbed, (C, D) Cs-Ze-Zr beads after nitrate adsorbed, (E, F) EDX of Cs-Ze-Zr composite beads and nitrate ion after adsorption on Cs-Ze-Zr respectively
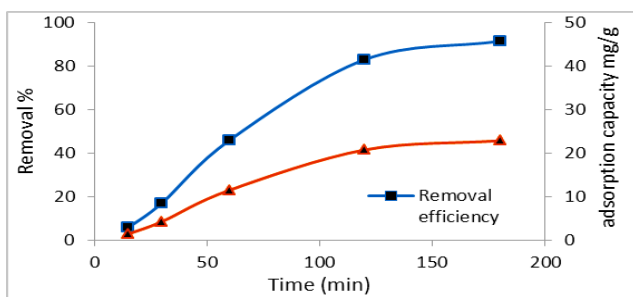

Fig. 6. Effect of contact time on removal efficiency and adsorption capacity

This behavior could be attributed to the abundance of unoccupied active sites in the initial stage of the process. Thereafter, the adsorption capacity is slightly restrained because of the adsorbates accumulation.[15] The results achieved in the current work agree with the results obtained by the literature.[27]

From this set of experiments, it can be concluded that the best operation time for the adsorption process is 120 minutes, were removal efficiency and adsorption capacity are at their adequate values; further increase in experimental time is impractical for the process. Consequently, the rest of the results are going to introduce at an operation time of 120 minutes.

3.6. Effect of Initial Concentration

Practically, the water resources content different concentration of pollutants. Therefore, it's crucial for any treatment method to examine the feasibility of a treatment system with different ranges of pollutant concentration. In the current study, the effect of NO_3 concentration on removal efficiency and adsorption capacity was examined in the range of 50–600 mg/L, with an adsorbent dosage of 0.1 g, rotation speed of 150 rpm, at a contact time of 120 minutes and ambient temperature. Fig. 7 demonstrates that the increase of pollutant concentration declines the removal efficiency. The removal efficiency decreases distinctly from 83.03% at a concentration of 50 mg/L to around 26.70 % at an initial NO_3 concentration of 600 mg/L.

On the other hand, the adsorption capacity shows a reverse response to that obtained with a removal efficiency. The adsorption capacity augmented dramatically from 20.7 mg/g with an initial concentration of 50 mg/L to around 80.12 mg/g with an initial NO_3 concentration of 600 mg/L.

This rise could be attributed to the increased driving power generated by the nitrate concentration gradient between the aqueous and solid phases.[42] The maximum adsorption capacity of 80.15 mg/g was achieved at concentrations of 400 mg/L. After that, the

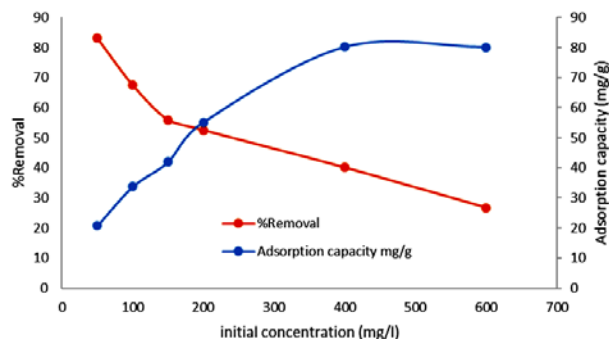adsorption capacity carves flattened, where the active sites of the adsorbed are saturated with the pollutant.

Fig. **7**. Effect of NO$_3$ concentration on removal efficiency and adsorption capacity

3.7. Effect of Adsorbent Dosage

By adjusting the dosage, the optimal adsorbent dosage may have been studied in the range of 0.05, 0.1, 0.2, and 0.3 g. The experimental conditions were the following: a contact time of 120 minutes, a rotational speed of 150 rpm, ambient temperature and a 50 mg/L nitrate solution. The removal of nitrate ions is illustrated by the dosage of the adsorbent in Fig. 8. The removal percentage augmented along with the increase in Cs-Ze-Zr dose. This upward tendency is brought on by a rise in active sites and functional groups available as a result of a rise in an adsorbent dosage. The adsorption process achieves the equilibrium point after a constant rise in the removal efficiency due to the overcrowding of adsorbent particles on adsorption sites.[43] As a result, the best dosage of 0.2 g was chosen for this research.
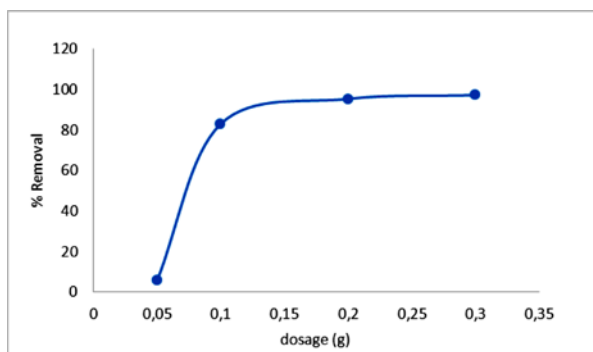

Fig. 8. Effect of adsorbent dosage on the removal efficiency

3.8. Adsorption Isotherm

Adsorption isotherms, graphs used to assess adsorption studies, were applied to investigate the adsorption mechanism and general efficacy (chemisorption/ physisorption). To ascertain the nitrate adsorption statics onto Cs-Ze-Zr beads, Temkin's isotherm models in addition to well-known isotherm models, including Freundlich and Langmuir ones, were examined.

3.8.1. Langmuir Isotherm Model

It is based on the assumption that the adsorbent has a constant adsorption energy at a constant temperature when the adsorbed solute forms a monolayer. Linear form is expressed as

$$\frac{1}{q_e} = \frac{1}{q_{max}} + \frac{1}{q_{max} k_L} \frac{1}{c_e} \qquad (3)$$

where q_e (mg/g) is the amount of nitrate adsorbed by adsorbent mass at equilibrium, c_e is the concentration of nitrate (mg/L), and k_L is Langmuir constant (L/mg). The q_{max} (mg NO$_3$/g adsorbent) is the maximal monolayer adsorption capacity. Additionally, it was possible to explain the Langmuir isotherm using the separation factor that was determined using Eq. (4):[44]

$$R_L = \frac{1}{1 + k_L c_i} \qquad (4)$$

where c_i is the initial concentration of nitrate (mg/L). R_L's value indicates the sort of isotherm, with $R_L = 0$ being irreversible, ($0 < R_L < 1$) being favorable, and $R_L = 1$ being unfavourable.

The plot of $1/q_e$ vs. $1/c_e$ is illustrated in Fig. 9, the q_{max} and k_L are computed from the slope and intercepted, respectively.

3.8.2. Freundlich Isotherm Model

The Freundlich model presupposed that the adsorption process takes place in a multilayer sorption and that the molecular distribution on the adsorbent surface is heterogeneous.[45] Freundlich's equation is illustrated below in its linear form:

$$\log q_e = \log k_f + \frac{1}{n} \log c_e \qquad (5)$$

where q_e (mg/g) is the amount of nitrate adsorbed by adsorbent mass at equilibrium, c_e is the concentration of nitrate (mg/L), Freundlich empirical constants K_F (mg/g) and n serve as an indicator of adsorption capacity and favorability. The plot of log q_e vs. log c_e is illustrated in Fig. 10. The $1/n$ and K_F are computed from the slope and intercepted, respectively.

3.8.3 Temkin Isotherm Model

One characteristic of the Temkin isotherm makes good quality of the interaction between the adsorbent and adsorbate. Forms using this model were used and provided as Eq. (6) below:

$$q_e = B \ln k_T + B \ln c_e \qquad (6)$$

where B is the Temkin constant and k_T is the Temkin isotherm constant (L/mg).

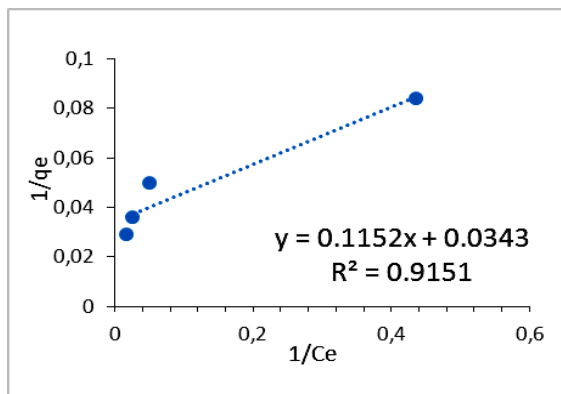The plot of q_e Temkin isotherm vs. ln c_e is illustrated in Fig. 11.
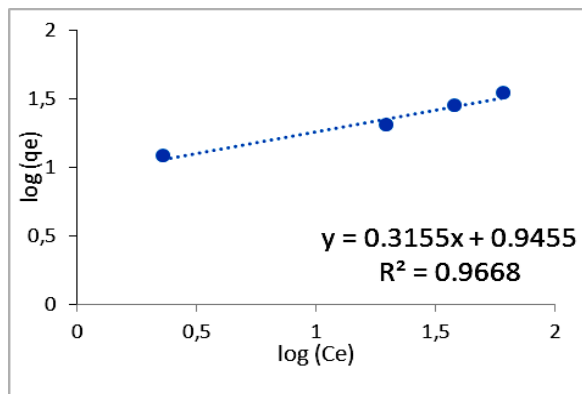
Fig. 9. Langmuir adsorption isotherm

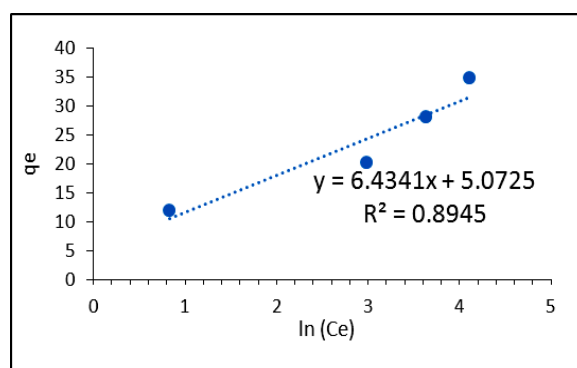Fig. 10. Freundlich adsorption isotherm

Fig. 11. Temkin adsorption isotherm

Table 1 shows the correlation coefficient R^2 for the Langmuir, Freundlich, and Temkin isotherm, which are (0.9151), (0.9668) and (0.8945), respectively. It amply demonstrates that the experimental data of nitrate ion adsorption by Cs-Ze-Zr are a decent fit with the Freundlich model.

Table 1. Parameter of Langmuir, Freundlich, and Temkin isotherm for nitrate ions

Isotherm	Parameter	Value
Langmuir	k_L	0.2977
	q_m	29.15
	R^2	0.9151
	R_L	0.0629
Freundlich	k_F	8.8206
	$1/n$	0.3155
	n	3.1695
	R^2	0.9668
Temkin	k_T	2.1998
	B	5.0725
	R^2	0.8945

The Freundlich coefficient n provides a measurement of the adsorption process favorability. The range of n values between 2 and 10 indicates the acceptable physical adsorption, between 1 and 2 – moderate difficulties, and below 1 – poor adsorption.[46,47] This was supported by the current study's n value (3.1695), which suggest massive physical adsorption.

3.9. Adsorption Kinetics

The pseudo-second-order and pseudo-first-order equations are two popular kinetic adsorption models that can calculate the adsorption rate. The tests were run in a variety of contact conditions over time. The linear form of the pseudo-first-order equation is as follows:

$$\ln(q_e - q_t) = \ln q_e - k_1 t \qquad (7)$$

where k_1 (L/min) is the pseudo-first-order constant; q_e and q_t (mg NO_3/g adsorbent) are the amounts of nitrate ions adsorbed at equilibrium and at any time, respectively. Fig. 1 shows the ln (q_e-q_t) vs. time graph.

The linear form of the pseudo-second-order equation shows:

$$\frac{t}{q_t} = \frac{1}{k_2 q_e^2} + \frac{t}{q_e} \qquad (8)$$

where k_2 (g/mg. min) is the pseudo-second-order constant. Fig. 13 shows the graph of t/q_t vs. time.
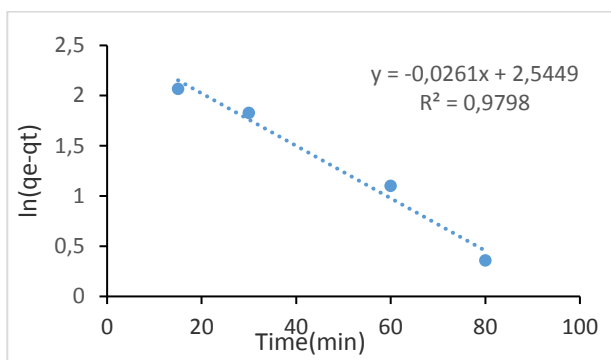
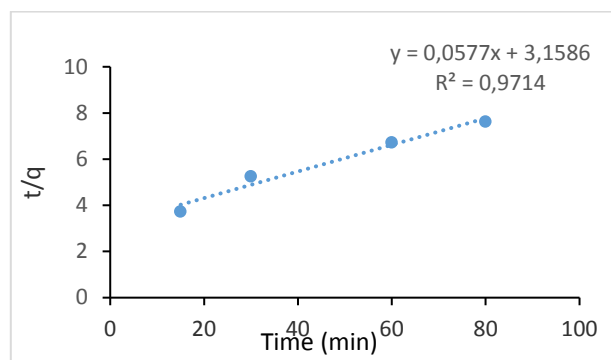Fig. 12. Pseudo-first-order kinetic model of nitrate ions

Fig. 13. Pseudo-second-order kinetic model of nitrate ions

According to Table 2, the correlation coefficients for the pseudo-first-order and pseudo-second-order were (0.9798) and (0.9714), respectively. These results showed that the pseudo-first-order model described the adsorption of nitrate ions by Cs-Ze-Zr. Competently, the $q_{e\ cal}$ for the pseudo-first-order (12.74 mg/g) was considerably more in line with the experimental value (11.9275 mg/g) than the pseudo-second-order.[48,49] The pseudo-first-order kinetic process indicates equilibrium between the liquid and solid phase for reversible reactions. At the same time, the pseudo-second-order kinetic model predicts that mass transfer is not the rate-limiting step but rather the adsorption mechanism.

Table 2. Parameters of pseudo-first-order and pseudo-second-order kinetics of nitrate ions

Kinetic Model	Parameter	Values	R^2
1st order	$q_{e\ cal}$ mg/g	12.74	0.9798
	$q_{e\ exp}$ mg/g	11.9275	
	k_1(1/min)	0.0261	
2nd order	$q_{e\ cal}$ mg/g	17.33	0.9714
	$q_{e\ exp}$ mg/g	11.9275	
	k_2 g/mg·min	$1.05 \cdot 10^{-3}$	

4. Conclusions

The removal of nitrate from water by modified (Cs-Ze-Zr) beads was investigated in this research. XRD, FTIR and FESEM have characterized the (Cs-Ze-Zr) bead. The key effective parameters were explored, and the results demonstrated that the best time of removal was 120 minutes, and the optimum dosage was 1g/250mL of Cs-Ze-Zr. The adsorption capacity increased with increasing the nitrate concentration while the removal efficiency decreased. In addition, by increasing the adsorbent dosage, the removal efficiency increased, and the adsorption capacity decreased. The maximum adsorption capacity for nitrate ions on Cs-Ze-Zr was 80.15 mg/g. Since the isotherm data for nitrate ions fit the Freundlich isotherm the best, it was clear that multilayer sorption predominated. Also, the adsorption kinetic for the nitrate ions followed the pseudo-first-order in kinetic experiments, showing that physical adsorption has prevailed. The current work's ultimate concentration of treated water reached the global limit of nitrate. Consequently, the Cs-Ze-Zr beads can be utilized for simple separation procedures, and it could be a useful solution to the real-world issues posed by separation processes.

References

[1]   Yang, K.; Yan, L.G.; Yang, Y.M.; Yu, S.J.; Shan, R.R.; Yu, H.Q.; Zhu, B.C.; Du, B. Adsorptive Removal of Phosphate by Mg-Al and Zn-Al Layered Double Hydroxides: Kinetics, Isotherms and Mechanisms. *Sep. Purif. Technol*. **2014**, *124*, 36–42. https://doi.org/10.1016/j.seppur.2013.12.042

[2]   Banu, H.T.; Karthikeyan, P.; Meenakshi, S. Zr^{4+} Ions Embedded Chitosan-Soya Bean Husk Activated Bio-Char Composite Beads for the Recovery of Nitrate and Phosphate Ions from Aqueous Solution. *Int. J. Biol. Macromol*. **2019**, *130*, 573–583. https://doi.org/10.1016/j.ijbiomac.2019.02.100

[3]   Kamaraj, R.; Pandiarajan, A.; Jayakiruba, S.; Naushad, M.; Vasudevan, S. Kinetics, Thermodynamics and Isotherm Modeling for Removal of Nitrate from Liquids by Facile One-Pot Electrosynthesized Nano Zinc Hydroxide. *J. Mol. Liq*. **2016**, *215*, 204–211. https://doi.org/10.1016/j.molliq.2015.12.032

[4]   Van Voorthuizen, E.M.; Zwijnenburg, A.; Wessling, M. Nutrient Removal by NF and RO Membranes in a Decentralized Sanitation System. *Water Res*. **2005**, *39*, 3657–3667. https://doi.org/10.1016/j.watres.2005.06.005

[5]   Kuokkanen, V.; Kuokkanen, T.; Rämö, J.; Lassi, U.; Roininen, J. Removal of Phosphate from Wastewaters for Further Utilization Using Electrocoagulation with Hybrid Electrodes - Techno-Economic Studies. *J. Water Process Eng*. **2015**, *8*, e50–e57. https://doi.org/10.1016/j.jwpe.2014.11.008

[6]   Raval, H.D.; Rana, P.S.; Maiti, S. A Novel High-Flux, Thin-Film Composite Reverse Osmosis Membrane Modified by Chitosan for Advanced Water Treatment. *RSC Adv*. **2015**, *5*, 6687–6694. https://doi.org/10.1039/c4ra12610f

[7]   Quan, X.; Ye, C.; Xiong, Y.; Xiang, J.; Wang, F. Simultaneous Removal of Ammonia, P and COD from Anaerobically Digested Piggery Wastewater Using an Integrated

Process of Chemical Precipitation and Air Stripping. *J. Hazard. Mater.* **2010**, *178*, 326–332. https://doi.org/10.1016/j.jhazmat.2010.01.083

[8]   Liou, Y.H.; Lo, S.L.; Lin, C.J.; Kuan, W.H.; Weng, S.C. Chemical Reduction of an Unbuffered Nitrate Solution Using Catalyzed and Uncatalyzed Nanoscale Iron Particles. *J. Hazard. Mater.* **2005**, *127*, 102–110. https://doi.org/10.1016/j.jhazmat.2005.06.029

[9]   Rashed, M.N. *Adsorption Technique for the Removal of Organic Pollutants from Water and Wastewater*, Ch. 7; IntechOpen: Rijeka, 2013. https://doi.org/10.5772/54048

[10]   Gumnitsky, J.; Sabadash, V.; Matsuska, O.; Lyuta, O.; Hyvlud, A.; Venger, L. Dynamics of Adsorption of Copper Ions in Fixed-Bed Column and Mathematical Interpretation of the First Stage of the Process. *Chem. Chem. Technol.* **2022**, *16*, 267–273. https://doi.org/10.23939/chcht16.02.267

[11]   Hammadi, A.; Shakir, I. Adsorption Behavior of Light Naphtha Components on Zeolite (5A) and Activated Carbon. *Iraqi J. Chem. Pet. Eng.* **2019**, *20*, 27–33. https://doi.org/10.31699/IJCPE.2019.4.5

[12]   Waleed Khalid, M.; D. Salman, S. Adsorption of Chromium Ions on Activated Carbon Produced from Cow Bones. *Iraqi J. Chem. Pet. Eng.* **2019**, *20*, 23–32. https://doi.org/10.31699/ijcpe.2019.2.4

[13]   Choudhary, V.R.; Vaidya, S.H. Adsorption of Copper Nitrate from Solution on Silica Gel. *J. Chem. Technol. Biotechnol.* **1982**, *32*, 888–892. https://doi.org/10.1002/jctb.5030320726

[14]   Hummadi, K.K. Optimal Operating Conditions for Adsorption of Heavy Metals from an Aqueous Solution by an Agriculture Waste. *Iraqi J. Chem. Pet. Eng.* **2021**, *22*, 27–35. https://doi.org/10.31699/ijcpe.2021.2.4

[15]   Karthikeyan, P.; Banu, H.A.T.; Meenakshi, S. Synthesis and Characterization of Metal Loaded Chitosan-Alginate Biopolymeric Hybrid Beads for the Efficient Removal of Phosphate and Nitrate Ions from Aqueous Solution. *Int. J. Biol. Macromol.* **2019**, *130*, 407–418. https://doi.org/10.1016/j.ijbiomac.2019.02.059

[16]   Hasmath Farzana, M.; Meenakshi, S. Photocatalytic Aptitude of Titanium Dioxide Impregnated Chitosan Beads for the Reduction of Cr(VI). *Int. J. Biol. Macromol.* **2015**, *72*, 1265–1271. https://doi.org/10.1016/J.IJBIOMAC.2014.09.029

[17]   Keshvardoostchokami, M.; Majidi, M.; Zamani, A.; Liu, B. A Review on the Use of Chitosan and Chitosan Derivatives as the Bio-Adsorbents for the Water Treatment: Removal of Nitrogen-Containing Pollutants. *Carbohydr. Polym.* **2021**, *273*, 118625. https://doi.org/10.1016/j.carbpol.2021.118625

[18]   Saheed, I.O.; Oh, W.-D.; Suah, F.B.M. Chitosan Modifications for Adsorption of Pollutants – A Review. *J. Hazard. Mater.* **2021**, *408*, 124889. https://doi.org/10.1016/j.jhazmat.2020.124889

[19]   Nitsae, M.; Madjid, A.; Hakim, L.; Sabarudin, A. Preparation of Chitosan Beads Using Tripolyphosphate and Ethylene Glycol Diglycidyl Ether as Crosslinker for Cr(VI) Adsorption. *Chem. Chem. Technol.* **2016**, *10*, 105–114. https://doi.org/10.23939/chcht10.01.105

[20]   Rajeswari, A.; Amalraj, A.; Pius, A. Removal of Phosphate Using Chitosan-Polymer Composites. *J. Environ. Chem. Eng.* **2015**, *3*, 2331–2341. https://doi.org/10.1016/j.jece.2015.08.022

[21]   Karthikeyan, P.; Banu, H. A. T.; Meenakshi, S. Removal of Phosphate and Nitrate Ions from Aqueous Solution Using La^{3+} Incorporated Chitosan Biopolymeric Matrix Membrane. *Int. J. Biol. Macromol.* **2019**, *124*, 492–504. https://doi.org/10.1016/j.ijbiomac.2018.11.127

[22]   Azlan, K.; Wan Saime, W.N.; Lai Ken, L. Chitosan and Chemically Modified Chitosan Beads for Acid Dyes Sorption. *J. Environ. Sci.* **2009**, *21*, 296–302. https://doi.org/10.1016/S1001-0742(08)62267-6

[23]   Kumar, I.A.; Viswanathan, N. Fabrication of Metal Ions Cross-Linked Alginate Assisted Biocomposite Beads for Selective Phosphate Removal. *J. Environ. Chem. Eng.* **2017**, *5*, 1438–1446. https://doi.org/10.1016/j.jece.2017.02.005

[24]   Kljajević, L.J.; Matović, B.; Radosavljević-Mihajlović, A.; Rosić, M.; Bosković, S.; Devečerski, A. Preparation of ZrO$_2$ and ZrO$_2$/SiC Powders by Carbothermal Reduction of ZrSiO$_4$. *J. Alloys Compd.* **2011**, *509*, 2203–2215. https://doi.org/10.1016/j.jallcom.2010.11.002

[25]   Wafiroh, S.; Abdulloh, A.; Widati, A.A. Phosphorylated Zeolite-A/Chitosan Composites as Proton Exchange Membrane Fuel Cell. *Chem. Chem. Technol.* **2018**, *12*, 229–235. https://doi.org/10.23939/chcht12.02.229

[26]   Kulprathipanja, S. *Zeolites in Industrial Separation and Catalysis*; 2010. https://doi.org/10.1002/9783527629565

[27]   Sowmya, A.; Meenakshi, S. Zr(IV) Loaded Cross-Linked Chitosan Beads with Enhanced Surface Area for the Removal of Nitrate and Phosphate. *Int. J. Biol. Macromol.* **2014**, *69*, 336–343. https://doi.org/10.1016/j.ijbiomac.2014.05.043

[28]   Alver, E.; Metin, A.; Çiftçi, H. Synthesis and Characterization of Chitosan/Polyvinylpyrrolidone/Zeolite Composite by Solution Blending Method. *J. Inorg. Organomet. Polym. Mater.* **2014**, *24*, 1048–1054. https://doi.org/10.1007/s10904-014-0087-z

[29]   Nathan, A. J.; Scobell, A. APHA AWWA 23rd EDITION; 2017; Vol. 91.

[30]   Thamilarasan, V.; Sethuraman, V.; Gopinath, K.; Balalakshmi, C.; Govindarajan, M.; Mothana, R.A.; Siddiqui, N.A.; Khaled, J.M.; Benelli, G. Single Step Fabrication of Chitosan Nanocrystals Using Penaeus Semisulcatus: Potential as New Insecticides, Antimicrobials and Plant Growth Promoters. *J. Clust. Sci.* **2018**, *29*, 375–384. https://doi.org/10.1007/s10876-018-1342-1

[31]   Zheng, H.; Han, L.; Ma, H.; Zheng, Y.; Zhang, H.; Liu, D.; Liang, S. Adsorption Characteristics of Ammonium Ion by Zeolite 13X. *J. Hazard. Mater.* **2008**, *158*, 577–584. https://doi.org/https://doi.org/10.1016/j.jhazmat.2008.01.115

[32]   Alshahidy, B.A.; Abbas, A.S. Preparation and Modification of 13X Zeolite as a Heterogeneous Catalyst for Esterification of Oleic Acid. *AIP Conf. Proc.* **2020**, *2213*, 020167. https://doi.org/10.1063/5.0000171

[33]   Thakkar, H.; Eastman, S.; Hajari, A.; Rownaghi, A. A.; Knox, J. C.; Rezaei, F. 3D-Printed Zeolite Monoliths for CO$_2$ Removal from Enclosed Environments. *ACS Appl. Mater. Interfaces* **2016**, *8*, 27753–27761. https://doi.org/10.1021/acsami.6b09647

[34]   Gorodylova, N.; Šulcová, P.; Bosacka, M.; Filipek, E. DTA-TG and XRD Study on the Reaction between ZrOCl$_2$·8H$_2$O and (NH$_4$)$_2$HPO$_4$ for Synthesis of ZrP$_2$O$_7$. *J. Therm. Anal. Calorim.* **2014**, *118*, 1095–1100. https://doi.org/10.1007/s10973-014-3890-4

[35]   Elanchezhiyan, S.S.; Sivasurian, N.; Meenakshi, S. Enhancement of Oil Recovery Using Zirconium-Chitosan Hybrid Composite by Adsorptive Method. *Carbohydr. Polym.* **2016**, *145*, 103–113. https://doi.org/10.1016/j.carbpol.2016.02.038

[36]   Yang, Z.; Peng, H.; Wang, W.; Liu, T. Crystallization Behavior of Poly(ε-Caprolactone)/Layered Double Hydroxide Nanocomposites. *J. Appl. Polym. Sci.* **2010**, *116*, 2658–2667. https://doi.org/10.1002/app.31787

[37]   De Lucas, A.; Uguina, A. M.; Covián, I.; Rodríguez, L. Synthesis of 13X Zeolite from Calcined Kaolins and Sodium Silicate for Use in Detergents. *Ind. Eng. Chem. Res.* **1992**, *31*, 2134–2140. https://doi.org/10.1021/ie00009a010

[38] Lechert, H.; Kacirek, H. The Kinetics of Nucleation of X Zeolites. *Zeolites* **1993**, *13*, 192–200. https://doi.org/10.1016/S0144-2449(05)80277-5

[39] Zhou, C.; Alshameri, A.; Yan, C.; Qiu, X.; Wang, H.; Ma, Y. Characteristics and Evaluation of Synthetic 13X Zeolite from Yunnan's Natural Halloysite. *J. Porous Mater.* **2013**, *20*, 587–594. https://doi.org/10.1007/s10934-012-9631-9

[40] Jiang, H.; Chen, P.; Luo, S.; Tu, X.; Cao, Q.; Shu, M. Synthesis of Novel Nanocomposite Fe₃O₄/ZrO₂/Chitosan and Its Application for Removal of Nitrate and Phosphate. *Appl. Surf. Sci.* **2013**, *284*, 942–949. https://doi.org/10.1016/j.apsusc.2013.04.013

[41] Nur, T.; Shim, W.G.; Loganathan, P.; Vigneswaran, S.; Kandasamy, J. Nitrate Removal Using Purolite A520E Ion Exchange Resin: Batch and Fixed-Bed Column Adsorption Modelling. *Int. J. Environ. Sci. Technol.* **2015**, *12*, 1311–1320. https://doi.org/10.1007/s13762-014-0510-6

[42] Liu, Q.; Hu, P.; Wang, J.; Zhang, L.; Huang, R. Phosphate Adsorption from Aqueous Solutions by Zirconium (IV) Loaded Cross-Linked Chitosan Particles. *J. Taiwan Inst. Chem. Eng.* **2016**, *59*, 311–319. https://doi.org/10.1016/j.jtice.2015.08.012

[43] Ali, M.E.A. Synthesis and Adsorption Properties of Chitosan-CDTA-GO Nanocomposite for Removal of Hexavalent Chromium from Aqueous Solutions. *Arab. J. Chem.* **2018**, *11*, 1107–1116. https://doi.org/10.1016/j.arabjc.2016.09.010

[44] Purbasari, A.; Ariyanti, D.; Sumardiono, S.; Khairunnisa, K.; Sidharta, T. Adsorption Kinetics and Isotherms of Cu(II) and Fe(II) Ions from Aqueous Solutions by Fly Ash-Based Geopolymer. *Chem. Chem. Technol.* **2022**, *16*, 169–176. https://doi.org/10.23939/chcht16.02.169

[45] Nuryanti, S.; Suherman; Rahmawati, S.; Amalia, M.; Santoso, T.; Muhtar, H. Langmuir and Freundlich Isotherm Equation Test on the Adsorption Process of Cu (II) Metal Ions by Cassava Peel Waste (*Manihot esculenta crantz*). *J. Phys. Conf. Ser.* **2021**, *2126*, 012022. https://doi.org/10.1088/1742-6596/2126/1/012022

[46] Radhi, B.D.; Mohammed, W.T. TiO₂ Loading on Activated Carbon: Preparation, Characterization, Desulfurization Performance and Isotherm of the Adsorption of Dibenzothiophene from Model Fuel. *Egypt. J. Chem.* **2022**. https://doi.org/10.21608/EJCHEM.2022.109702.5003

[47] Li, M.; Lu, B.; Ke, Q.-F.; Guo, Y.-J.; Guo, Y.-P. Synergetic Effect between Adsorption and Photodegradation on Nanostructured TiO₂/Activated Carbon Fiber Felt Porous Composites for Toluene Removal. *J. Hazard. Mater.* **2017**, *333*, 88–98. https://doi.org/https://doi.org/10.1016/j.jhazmat.2017.03.019

[48] Jawad, R.J.; Ismail, M.H.S.; Siajam, S.I. Adsorption of Heavy Metals and Residual Oil from Palm Oil Mill Effluent Using a Novel Adsorbent of Alginate and Mangrove Composite Beads Coated with Chitosan in a Packed Bed Column. *IIUM Eng. J.* **2018**, *19*, 1–14. https://doi.org/10.31436/iiumej.v19i1.734

[49] Malekbala, M.R.; Soltani, S.M.; Yazdi, S.K.; Hosseini, S. Equilibrium and Kinetic Studies of Safranine Adsorption on Alkali-Treated Mango Seed Integuments. *Int. J. Chem. Eng. Appl.* **2012**, *3*, 160–166. https://doi.org/10.7763/ijcea.2012.v3.179

ПАРАМЕТРИЧНЕ ТА КІНЕТИЧНЕ ДОСЛІДЖЕННЯ ВИДАЛЕННЯ НІТРАТІВ З ВОДИ МОДИФІКОВАНИМИ КОМПОЗИТНИМИ КУЛЬКАМИ З ХІТОЗАНУ

Анотація. *Забруднення водних об'єктів шкідливими забруднюючими речовинами є однією з найгостріших глобальних проблем. Поточне дослідження зосереджено на розробці ефективного адсорбенту для видалення нітрат-іонів з водних розчинів. У дослідженні запропоновано модифіковані композитні хітозан-цеолітні кульки для підвищення ефективності процесу адсорбції. Цеоліт використовували для збільшення площі поверхні, а цирконій наносили на кульки для підвищення селективності щодо нітрат-аніонів. Механізм адсорбції оцінювали, характеризуючи вихідні кульки та кульки з адсорбованим сорбатом за допомогою рентгеноструктурного аналізу (XRD), інфрачервоної спектроскопії з перетворенням Фур'є (FTIR), польової емісійної сканувальної електронної мікроскопії (FESEM) та аналізу за допомогою енергодисперсійного рентгенівського аналізатора (EDX). Досліди проводили в системі періодичної дії та вивчали вплив ключових параметрів, таких як час контакту, початкова концентрація нітрат-аніонів і дозування адсорбенту на ефективність адсорбції. Результати показали, що найвищий ступінь вилучення нітрат-іонів був зафіксований на рівні 95,42 % за використання 0,2 г Cs-Ze-Zr адсорбенту з початковою концентрацією 50 мг/л і часом контакту 120 хвилин. Максимальна адсорбційна здатність щодо нітрат-іонів на виготовленій кульці становила 80,15 мг/г. Крім того, серед ізотерм Фрейндліха, Ленгмюра і Темкіна дані про рівновагу ізотерми узгоджувалися з моделлю ізотерми Фрейндліха. Кінетичні дані для адсорбції були задовільно апроксимовані псевдопершим порядком. Отримані результати чітко вказують на те, що запропонований адсорбент (Cs-Ze-Zr) може бути успішно використаний для вилучення нітрат-іонів, що підтверджується високою ефективністю вилучення й адсорбційною здатністю, отриманою в дослідженні.*

Ключові слова: *модифікований хітозан, періодична адсорбція, нітрат, цеоліт, цирконій.*